Journal of Institute of Science and Technology, 30(2), 93-104 (2025)
ISSN: 2467-9062 (print), e-ISSN: 2467-9240
https://doi.org/10.3126/jist.v30i2.84993

Research Article

THERMODYNAMIC BEHAVIOR, DIFFUSION MECHANISMS AND STRUCTURAL PROPERTIES OF PANOBINOSTAT IN WATER

Narayan Gautam[1,2], Deependra Awasthi[1], Shyam P. Khanal[1*], Rajendra P. Koirala[1*], Narayan P. Adhikari[1]
[1]Central Department of Physics, Tribhuvan University, Kirtipur, Kathmandu, Nepal
[2]Tri-Chandra Multiple Campus, Tribhuvan University, Ghantaghar, Kathmandu, Nepal
[*]Correspondence:shyamkhanal1989@gmail.com; rajendra.koirala@cdp.tu.edu.np

***(Received:** October 1, 2025; **Revised:** November 17, 2025; **Accepted:** November 23, 2025)*

ABSTRACT

Panobinostat is used as a drug against multiple myeloma by inhibiting the enzymatic activity of HDAC enzymes. In this study, we have performed molecular dynamics simulation of Panobinostat in water at 310 K to investigate solvation free energy, diffusion mechanism and structural properties. TI, TI-CUBIC, BAR and MBAR have been used to estimate solvation free energy. Our findings indicate that Coulomb interaction is the dominant factor affecting solute solvation free energy. We have also investigated the solute-solvent interactions in terms of solvent accessible surface area (SASA) of solute molecule, and hydrogen bonds between the Panobinostat and water. Solute-solvent interaction revealed a mean SASA of 6.64 nm^2 with an average of 6 hydrogen bonds between Panobinostat and water. The calculated self-diffusion coefficient of water agreed well with literature values within 4.26% deviation. Both bulk and shear viscosity significantly exceeded than pure water, indicating a viscous micro-environment around Panobinostat. Moreover, structural properties of the system have been analyzed using radial distribution function (RDF).

Keywords: HDACs inhibitors, Panobinostat, Solvation Free Energy, Diffusion, SASA

INTRODUCTION

Histone deacetylases (HDACs) control protein acetylation and are involved in numerous biological functions, such as DNA replication and repair, chromatin remodeling, gene expression. Overexpression of HDAC proteins is associated with multiple myeloma (MM). Histone deacetylase inhibitors are anticancer drugs that exhibit potent antitumor activity by controlling transcriptional activities associated with cell growth arrest, proliferation, and death (Bolden *et al.*, 2006). HDAC inhibitors (HDACi) inhibit various types of cancer. One of the important HDACi is Panobinostat. It is an inhibitor of HDACs, inhibits the activities of class I HDACs, class II HDACs, and class IV HDAC proteins. The United States of America (USA), Food and Drug Administration (FDA) has approved different HDACi such as vorinostat, romidepsin for different cancers and Panobinostat for multiple myeloma (Administration, 2014; Gryder *et al.*, 2012). Aside from Panobinostat, many hydroxamic acid derivatives are recognized as HDACi, including Resminostat, Givinostat, Abexinostat, Pracinostat, and Quisinostat, that are currently undergoing clinical trials for various types of cancer (Rajak *et al.*, 2014).

Panobinostat inhibits class I, II, and IV HDAC enzymatic activities, that increases histone acetylation than other HDAC inhibitors (Kusaczuk *et al.*, 2016; San José-Enériz *et al.*, 2019). This extensive hyperacetylation disrupts a variety of biological phenomenon in cells, including transcriptional activity and survival mechanisms. It was first approved for multiple myeloma in 2015, has shown significant promise in preclinical studies for the treatment of Acute Lymphocytic Leukemia (ALL) (Pan *et al.*, 2023; Raedler, 2016; Sivaraj *et al.*, 2016). It has been shown to induce apoptosis and make other treatments, like bortezomib, work better in leukemia by important mechanism (Jiang *et al.*, 2012). It has also been tested in clinical trials to see how well it works in overcoming drug resistance and stopping the disease from coming back in leukemia patients (Morabito *et al.*, 2016). It belongs to the hydroxamic acid class of HDACi. It was approved by the US FDA to treat multiple myeloma.

Panobinostat contains 26 heavy atoms having molecular weight 349.4 g/mol with no net charge. It is marginally soluble in water and its solubility is pH dependent with highest solubility around pH 3.0 (Rodgers *et al.*, 2020). The water solubility of Panobinostat is 0.00198 mg/mL (Knox *et al.*, 2024). Panobinostat is a colorless, clear, slightly viscous liquid that can be taken orally or intravenously (Administration, 2014; Giles *et al.*, 2006). The

chemical formula of Panobinostat is C21H23N3O2 and IUPAC name is (2*E*) − *N* − *hydroxy* − 3 − [4 − ([2 − (2 − *methyl* − 1*H* − *indol* − 3 – *yl*) *ethyl*] *aminomethyl*) *phenyl*] *acrylamide*. The molecular structure of the Panobinostat is shown in Figure 1.

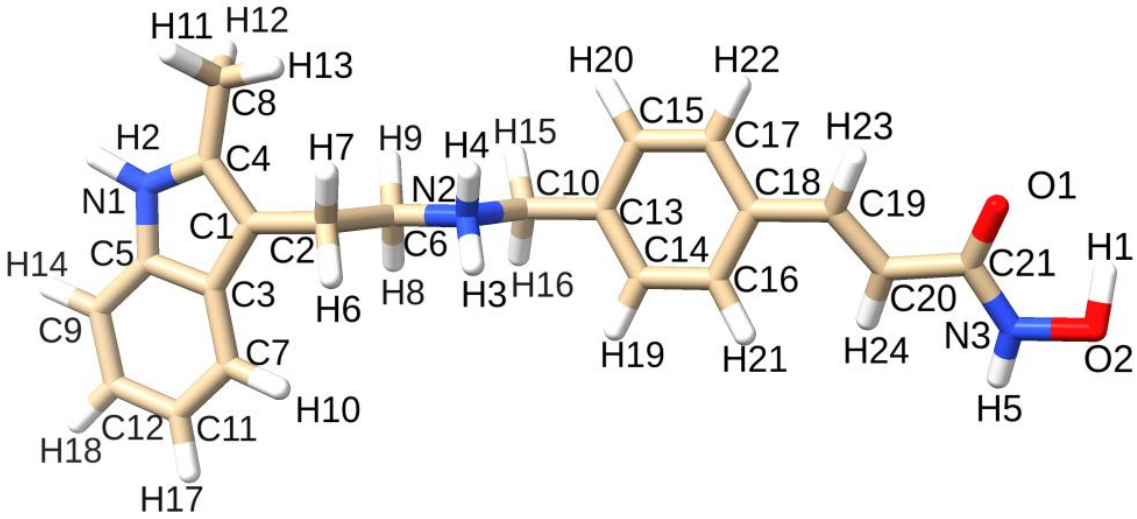

Figure 1: Molecular structure of Panobinostat.

It is useful in certain types of cancer and has also been proposed in the treatment of HIV infection (Tsai *et al.*, 2016). This hydroxamic acid-based HDACi has been tested on different types of cancer. They are in clinical trials and being developed for several cancers, including CTCL, lymphoma, leukemia, prostate, thyroid, breast, and other blood-related and solid tumors (Jones *et al.*, 2011). Panobinostat causes prolonged hyperacetylation of the histone protein and modulates gene expression more prominently in tumor cells than in healthy cells. Many factors influence drug distribution to the brain, including drug molecule size, drug charge and tissue affinity or binding, and drug water solubility (Bobo *et al.*, 1994; Gill *et al.*, 2013; Morrison *et al.*, 1994). Drug discovery requires understanding of the solvation properties of the targeted molecule. It provides insight into the bio-activity of the drug candidate at the site of action. Understanding the solvation free energy is important in the early stages of drug discovery (Kraml *et al.*, 2019). In addition, Panobinostat is an oral accessible pan-HDAC inhibitor that is to be administered to various cells throughout the body, primarily in the brain and other nervous systems (Homan *et al.*, 2021). Estimation of the diffusion rate is crucial for studying the transportation of this molecule in the aqueous environment, which motivated us to investigate the diffusion of Panobinostat in water medium.

MATERIALS AND METHODS

Theoretical Background

The deterministic molecular dynamics (MD) is used to investigate the macroscopic properties of molecular system through the statistical mechanics by analyzing the trajectories of the particles (Allen & Tildesley, 2017; Karplus & Petsko, 1990). MD is an extremely useful method for investigating protein-protein interactions, drug discovery, and many other applications (De Vivo *et al.*, 2016). Utilizing MD simulation, we estimated solvation free energy as well as diffusion coefficient.

Free Energy of Solvation

Out of many computational approaches, Free Energy Perturbation (FEP) and Thermodynamic Integration (TI) based methods are widely used to estimate the free energy difference between two thermodynamic states. Solvation free energy calculated from alchemical free energy calculations are most consistently reliable methods in recent applications in modeling of protein and ligands (Bannan *et al.*, 2016; Geballe *et al.*, 2010; Guthrie, 2009; Liu *et al.*, 2016). Zwanzig introduced the exponential averaging also known as Free Energy Perturbation (Bhatta *et al.*, 2023; Khanal & Adhikari, 2022; Zwanzig, 1954). Free energy quantifies usable energy of the system for the work (Shirts & Chodera, 2008; Zwanzig, 1954).

Consider two thermodynamic states: initial state ‘X’ and final state ‘Y’ defined by potential energy U_X and

U_Y respectively. According to free energy perturbation (FEP) approach, the difference of free energy between the two states 'X' and 'Y' at temperature 'T' can be estimated using (Tuckerman, 2023):

$$\Delta F_{XY} = -k_B T \ln\langle exp\{-\beta(U_Y - U_X)\}\rangle_X \quad (1)$$

Where, $\beta = \frac{1}{k_B T}$ and $\langle - - - \rangle_X$ represents averaging over state X, enabling incremental computation of ΔF_{XY} by simulating small changes in potential energy. This equation is precise in the context of a large sample size; however, exponential averaging is inefficient. This leads to unstable free energy estimations and significant biases when configurations sampled in one state are highly unlikely in the alternate state, and vice versa. The phase space overlap between the two states is the probability that characterizes this likelihood (Liu *et al.*, 2016; Shirts *et al.*, 2007; Shirts & Pande, 2005). To enhance the significant phase-space overlapping, we use the intermediate states that boost the precision and robustness of the estimated free energy difference (Wu & Kofke, 2005). Moreover, we used thermodynamic integration (TI) method to calculate the free energy difference ΔF_{XY} by integrating the ensemble-averaged derivative of the potential energy ($\langle \partial U/\partial \lambda \rangle$) along a coupling parameter λ (with values $0 \leq \lambda \leq 1$):

$$\Delta F_{XY} = \int_0^1 \left\langle \frac{\partial U}{\partial \lambda} \right\rangle_\lambda d\lambda \quad (2)$$

Thermodynamic integration is typically implemented computationally by performing numerical quadrature on simulation data obtained at discrete λ values. The value of λ is 0 and 1 that denote the initial and final thermodynamic states respectively, with intermediate λ values between 0 and 1, representing intermediate transition states. This approach helps for free energy calculations by constructing a continuous thermodynamic pathway through systematic sampling of intermediate configurations. Both methodologies employ statistical mechanical principles used in computational simulations to compute free energy differences that provides crucial thermo- dynamic insights into molecular systems.

Diffusion Coefficient

Diffusion is the movement of atoms or particles from an area of high concentration to an area of low concentration caused by random motion (Rapaport, 2004). Such process is involved in a number of biochemical processes, including protein aggregation and transportation in intercellular media (Georgalis *et al.*, 1998; Krewson & Saltzman, 1996). It plays a key role in various physiological processes, such as biomolecule dynamics, nutrient transport, and drug distribution in the body (Bhandari & Adhikari, 2016). Diffusion is quantified using the diffusion coefficient, which measures how quickly particles move through a medium. Diffusion coefficient depends on different factors such as temperature and particle size (Allen & Tildesley, 2017; Khanal *et al.*, 2019). Using the mean squared displacement (MSD) $\langle r^2(t) \rangle$, the self-diffusion coefficient can be calculated via Einstein's relation (Einstein, 1905);

$$D = \frac{1}{6t} \lim_{t \to \infty} \left[r_\beta(t + t_0) - r_\beta(t_0) \right]^2 \quad (3)$$

where, β indicates particle type, and $\langle \text{---} \rangle$ represents an ensemble average. Moreover, the binary diffusion coefficient D_{XY} is given by Darken's relation (Darken, 2010):

$$D_{XY} = N_Y D_X + N_X D_Y \quad (4)$$

where, D_X and D_Y are the self-diffusion coefficients of X and Y, and N_X, N_Y are their mole fractions.

Shear Viscosity

Shear viscosity, also referred to as apparent viscosity, describes the proportionality between shear stress and shear rate in a fluid, remaining constant for Newtonian fluids as described by Newton's Law of Viscosity (Rah & Eu, 1999). In molecular simulations, shear viscosity can be calculated from equilibrium data using the Einstein relation (Hess, 2002):

$$\eta = \frac{1}{2} \frac{V}{k_B T} \lim_{t \to \infty} \langle \left(\int_0^{t_0 + t} P_{xz}(t')\, dt' \right)^2 \rangle_{t_0} \quad (5)$$

Here, η denotes shear viscosity, V the system volume, T the temperature, k_B the Boltzmann constant, and $P_{xz}(t')$ the off-diagonal component of the pressure tensor. The brackets $\langle ... \rangle_{t_0}$ represent an average over time origins. Although this method is straightforward, it is computationally expensive and converges slowly. Moreover, the treatment of electrostatics especially the use of short-range cut-offs can introduce significant noise into the pressure tensor, potentially inflating the calculated viscosity by an order of magnitude (Hess, 2002; Maginn *et al.*, 2019).

Computational Details

System Preparation

We used CHARMM-GUI web server (Lee *et al.*, 2016) to prepare the system for Panobinostat by using the sdf from PubChem Identifier: CID 6918837 (Kim *et al.*, 2025). Charmm36m force fields (Huang *et al.*, 2017) was used to model the system at pH 7.0. The Panobinostat was solvated using the TIP3P water model in a cubic box and neutralized with 150 mM NaCl. The solvated and neutralized system consists of 5527 atoms in a cubic simulation box. All simulations were carried out at 310 K under periodic boundary conditions (PBC) at 1 atm pressure using GROningen MAchine for Chemical Simulations (GROMACS) software package (Van Der Spoel *et al.*, 2005). To eliminate van der Waals bad contacts, we carried out

an energy minimization using the steepest descent method (Van Der Spoel *et al.*, 2005).

Estimation of Solvation Free Energy

In FEP method, free energy difference between two consecutive states becomes converge when there is sufficient overlapping of phase space in the states. For the substantial overlap between two states, we used smaller λ-intervals to improve sampling.

In contrast, TI method estimates the free energy by integrating the ensemble-averaged derivative of potential energy of the system with respect to a coupling parameter λ. We required multiple intermediate λ-values to ensure a smooth and accurate integration. For this, we select sufficient phase space sampling. In the case of our system, we introduced intermediate states by adjusting only the non-bonded vdW and Coulomb interactions and kept the bonded interactions unchanged. We use 21 evenly spaced values of the coupling parameter lambda to gradually change the system from its starting state to its final state.

For Coulomb interaction, $\lambda_{Coulomb}$ = 0.00, 0.10, 0.20, 0.30, 0.40, 0.50, 0.60, 0.70, 0.80, 0.90, 1.0,
1.00, 1.00, 1.00, 1.00, 1.00, 1.00, 1.00, 1.00, 1.00 and 1.00 and λ_{vdW} = 0.00, 0.00, 0.00, 0.00, 0.00, 0.00, 0.00, 0.00, 0.00, 0.00,0.00, 0.10, 0.20, 0.30, 0.40, 0.50,
0.60, 0.70, 0.80, 0.90 and 1.00 for van der Waals interaction. The initial state λ = 0 signifies complete coupling between the solute and solvent through non-bonded Coulomb and vdW interactions; final state λ = 1 denotes decoupling; and other intermediate states denote variations in the strength of the coupling.

To maintain thermodynamic equilibrium, we conducted a 2 ns equilibration run with a 1 fs time step, starting with the NVT ensemble and then switching to the NPT ensemble. During each equilibration phase, we used the LINCS algorithm to constrain all bonds and applied Langevin dynamics to integrate the equations of motion (Apol *et al.*, 2010; Hess, 2002). A Berendsen barostat was employed with a coupling time of 0.5 ps and an isothermal compressibility of 4.5 × 10^{-5} bar (Parrinello & Rahman, 1981). Initial particle velocities were assigned based on the Maxwell-Boltzmann distribution (Hess *et al.*, 1997). For non-bonded interactions, a cutoff of 1.4 nm was used, and long-range Coulomb interactions, along with Lennard-Jones and short-range Coulomb forces, were calculated using the Particle Mesh Ewald (PME) method. After equilibration, a 5 ns production run was carried out with a 2 fs time step using Langevin dynamics and the same parameters as in the equilibration run (Hess *et al.*, 1997). VMD and ChimeraX were used for converting SDF files to PDB format, visualizing molecular structures, performing structural analysis, and generating high-quality images (Humphrey *et al.*, 1996; Pettersen *et al.*, 2021).

Estimation of Diffusion Coefficient

To investigate diffusion coefficient, we conducted molecular dynamics (MD) simulations of mixture of Panobinostat and water. After system set up, we first conducted energy minimization run. Then the system was equilibrated at temperature of 310 K under isothermal-isobaric (NPT) ensemble conditions, employing a 2 fs time step for a duration of 100 ns using Leap-frog integration algorithms (Apol *et al.*, 2010). The Particle Mesh Ewald (PME) method is a computational technique used to calculate long-range Coulomb interactions between charged particles in systems like molecular dynamics simulations and employing 1 nm cutoff threshold for both Coulomb and Lennard-Jones interactions. Initial particle velocities were distributed according to the Maxwell-Boltzmann distribution, and all molecular bonds were constrained using the Linear Constraint Solver (LINCS) algorithm (Hess *et al.*, 1997). To control the temperature, velocity rescaling thermostat with a coupling time of 0.01 ps, while pressure was maintained via a Berendsen barostat with a coupling time of 0.8 ps was used (Berendsen *et al.*, 1984; Bussi *et al.*, 2007). Finally, we performed production run for the equilibrated system at temperature 310 K under canonical ensemble (NVT) conditions. We performed 500 ns MD simulation with a 2fs time step, maintaining identical parameters to those employed during the equilibration run.

RESULTS AND DISCUSSION

This investigation elucidates the essential thermodynamic and transport properties of Panobinostat in water as a solvent, particularly quantifying its solvation free energy, self-diffusion coefficient of solute as Panobinostat and solvent along with their diffusion coefficients. The physicochemical characterizations collectively improve our understanding of Panobinostat's behavior in biological systems and may inform future pharmaceutical development strategies to optimize its therapeutic efficacy.

Free Energy of Solvation

The solvation free energy of Panobinostat in water at a temperature of 310 K has been estimated by analyzing the simulation data obtained from the production runs carried out each value of lambda. To compute the solvation free energy several methods were used, including TI (with linear and cubic interpolation), FEP, and statistical estimators like BAR and MBAR. During our simulations, non-physical intermediate

states between the totally coupled and decoupled endpoints introduced through potential, also a function of coupling parameter (λ) to facilitate analysis. Our protocol included 21 different states, from the initial state (characterized by complete solute-solvent interaction through non-bonded van der Waals (vdW) and Coulomb interactions) to the final state (defined by complete absence of solute-solvent interaction). The free energy difference has been subsequently calculated by integrating the ensemble average of the free energy derivative with respect to lambda across all coupling states. Figure 2 shows the changes of $\left\langle \frac{\partial u}{\partial \lambda} \right\rangle_\lambda$ with λ for Panobinostat taking TIP3P water model as solvent at temp 310 K.

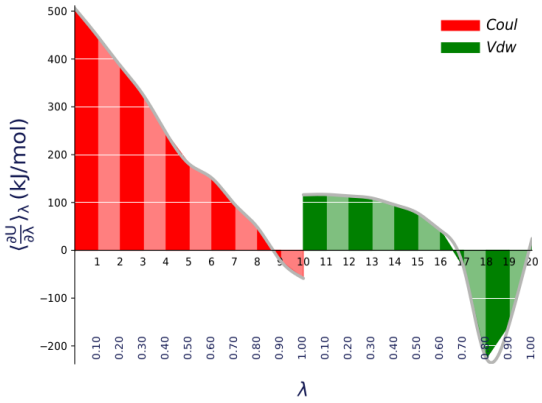

Figure 2: Variation of $\left\langle \frac{\partial u}{\partial \lambda} \right\rangle_\lambda$ with λ for Panobinostat taking TIP3P water model as solvent at temp 310 K.

In the Figure 2, red and green colors (online) indicate the contributions due to Columbic as well as van der Waals interactions respectively. These interactions are critical for the solvation free energy. In the simulations, the Coulomb interaction was turned off first, followed by the vdW interaction. The plot indicates that the free energy difference between consecutive coupling states is larger at the beginning than in subsequent states, a result of the decreasing coupling parameter. Initially, the solute-solvent interactions are at full strength and are gradually eliminated. The total free energy difference between the fully coupled initial state and the fully decoupled final state defines the solute's solvation free energy. Table 1 represents the calculated solvation free energy of Panobinostat in water at 310 K using four methods: TI, TI-CUBIC, BAR, and MBAR.

Table 1: Estimated values of free energy of solvation (ΔG_{solv}) for Panobinostat in TIP3P water at 310 K using TI, TI-CUBIC, BAR, and MBAR methods.

Interactions	ΔG_{sol} in kJ/mol estimated using method			
	TI	TI-CUBIC	BAR	MBAR
Coulomb	207.95 ± 0.66	207.69 ± 0.65	207.63 ± 0.43	207.99 ± 0.54
vdW	20.83 ± 0.33	19.27 ± 0.32	20.05 ± 0.33	20.16 ± 0.36
Total	228.78 ± 0.74	226.97 ± 0.73	227.68 ± 0.54	228.15 ± 0.65

Contribution of coulomb and vdW interactions to the solvation free energy using four different methods are about 208 kJ/mol and 20 kJ/mol respectively are shown in Table 1. Positive value of individual interactions indicating that both Coulomb as well as vdW contribute to the solvation of Panobinostat in water. The high positive value of Coulombic contribution (208 kJ/mol) suggests that there are strong electrostatic interactions, which typically increase water solubility. Panobinostat exhibits weaker van der Waals forces (19- 21 kJ/mol) than the Coulomb force. Moreover, our estimated values of solvation free energy for Panobinostat molecule in water using TI, TI-CUBIC, BAR and MBAR are in closed agreement (227-229 kJ/mol) that ensures the reliability of our calculations. This comprehensive analysis of solvation

free energy will be supported to understand the binding mechanisms and efficacy of HDACs inhibitors for potential drug optimization. To check the convergence, free energy difference as a function of simulation time for both forward and time-reversed plot is shown in Figure 3

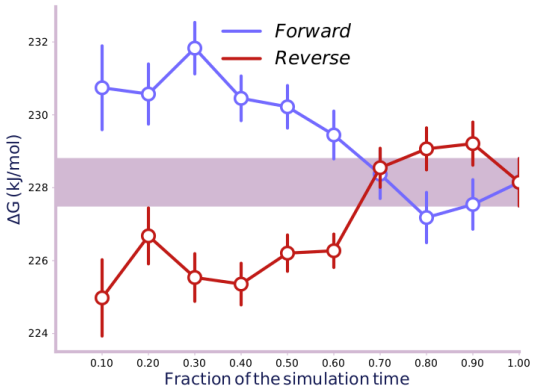

Figure 3: A convergence plot showing how well the forward and backward converged during the simulation of Panobinostat in TIP3P water.

The convergence plot shows the free energy difference of Panobinostat as a function of simulation time at 310 K temperature taking water as solvent. The forward estimation in blue line starts at about 230.5 kJ/mol, peaks around 232 kJ/mol at the 0.3 simulation fraction, and then gradually decreases until it reaches a minimum near 227.5 kJ/mol at the 0.8 fraction. The reverse estimation in red line begins at about 225 kJ/mol, then follows an irregular path with multiple local peaks before rising to converge with the forward calculation in the simulation. The purple band between 227.5 and 228.5 kJ/mol represents the convergence region where both calculations approach similar values. The convergence around the 0.7-1.0 fraction indicates that the simulation has likely completed enough sampling to provide a reliable free energy estimation. The final convergence value of 228 kJ/mol (±0.5 kJ/mol) is consistent with the total energy values in Table 1 (228 kJ/mol), validating the computational approach.

Hydrogen Bonds and Solvent Accessible Surface Area

Hydrogen bonds between the drug molecule and the solvent molecule ensure the stability of drug in the cellular environment. The orientation and distance of atoms in a drug molecule from the solvent molecule determine the strength of binding and stability of such a molecule in water. The hydrogen bonding energy needs to be considered while evaluating the effectiveness of drug. In this study, we analyzed the hydrogen bonds between Panobinostat and water molecules using the trajectory from the production run at the initial coupling state, represented by lambda = 0. Hydrogen bonds were estimated based on specific distance and angle criteria, using a cutoff of 0.35 nm for distance and 30° for angle. Figure 4(a) shows the number of hydrogen bonds between Panobinostat and water changes over simulation time at 310 K. This analysis also provides insights into the influence of the solvent environment. Our results show that up to 13 hydrogen bonds formed between Panobinostat and water during the simulation, with an average of 6 hydrogen bonds, indicating good solubility of Panobinostat in water.

The structure and function of biological molecules are significantly affected by their solvent accessibility. The nature of the amino acids on the surface of protein primarily determines its active sites. The dominance of hydrophobic residues on protein surfaces reduces solvent accessible surface area (SASA), whereas the hydrophilic character of amino acids on the surfaces increases SASA (Gromiha & Ahmad, 2005). Thus, SASA of present system measures how easily a Panobinostat can dissolve in water as a solvent. We have estimated the value of SASA of Panobinostat in water using the trajectory of production run for coupling state between solute as Panobinostat and solvent as water for lambda = 0. From Figure 4(b), it has been observed that the maximum and minimum value of SASA during time evolution are 7.58 nm^2 and 5.41 nm^2 respectively. The average value of SASA is about 6.64 nm^2 of Panobinostat in water throughout the simulation.

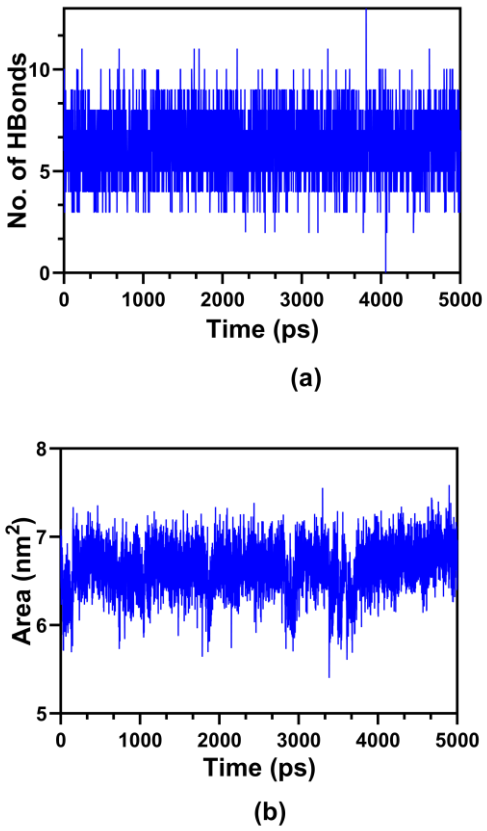

Figure 4: Time evolution of (a) Number of Hydrogen Bonds, and (b) Solvent Accessible Surface Area (SASA).

Diffusion Coefficient

We have estimated the self-diffusion coefficient of both the solute and solvent molecules as well as their binary diffusion coefficient at 310 K temperature using Einstein's and Darken's relations 3 and 4 respectively. Self-diffusion coefficient can be estimated from the slope of mean squared displacement (MSD) versus time. To find diffusive regime, we first plotted the variation of MSD as a function of time in logarithmic scale. It has observed that the graph becomes straight line after ballistic regime and slope of the straight line gives self-diffusion coefficient. We plotted MSD versus time graph for both the solute and solvent. The slope of the MSD versus time curve to measure diffusion of water and solute molecules are 40.50×10^{-9} m^2/s and 5.85×10^{-9} m^2/s respectively. From these numerical values of slope of MSD, we can say that solute molecules are significantly larger and less mobile than water molecules, as evidenced by their ~7 times lower diffusion coefficient. Although we performed 10 ns simulation, the plots are fitted linearly taking beginning portion of the trajectory for better statistics as shown in Figure 5.

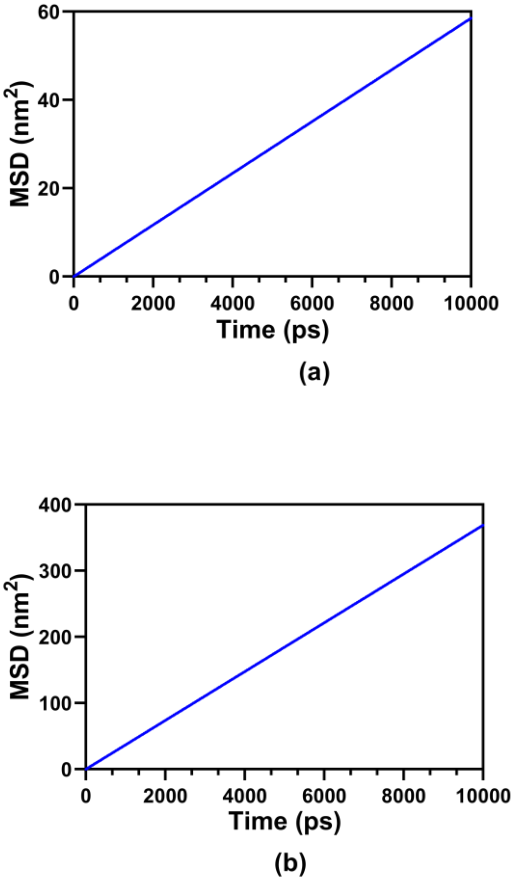

Figure 5: Linearly fitted mean squared displacement versus time plot for (a) Panobinostat, and (b) Water at 310 K.

The estimated self and binary diffusion coefficients at 310 K are shown in Table 2. The simulated self-diffusion coefficient of water closely matches previously reported values, differing by just 4.26%. Table 2 shows that the estimated binary diffusion coefficient of the system is nearly equal to the self-diffusion coefficient of the solute. This is due to infinite dilution of the system.

Table 2: Self diffusion coefficients of Panobinostat and water molecules as well as their binary diffusion coefficient at 310 K temperature.

Diffusion coefficient ($\times 10^{-9}$ m2/s) at 310 K temperature				
Self				Binary
Panobinostat	Water			
Estimated	Estimated	Ref. (Rosas Jiménez *et al.*, 2024)	% Error	Estimated
0.975	6.75	7.05	4.26	0.978

Shear Viscosity

The presented graph illustrates the time evolution of shear viscosity, bulk viscosity, and their average for the Panobinostat-water system over a simulation period of approximately 220,000 picoseconds (ps). The shear viscosity curve (green) remains relatively stable, fluctuating between 0.004 $kgm^{-1}s^{-1}$ to 0.010 $kgm^{-1}s^{-1}$, showing moderate and consistent resistance to shear deformation. In contrast, the bulk viscosity (orange) displays larger fluctuations with notable peaks, particularly beyond 150,000 ps, peaks above 0.018 $kgm^{-1}s^{-1}$, indicating dynamic structural changes or localized compressional resistance within the system. The average viscosity (red) lies between the two, reflecting a smoothed representation of the system's viscous behavior. The clear temporal fluctuations, followed by relative stabilization, suggest that the system reaches equilibrium over time, with viscosity values converging to physically meaningful averages. The data derived from this graph provides deeper insight into the intermolecular interactions and solvent structuring caused by Panobinostat in water. The relatively high and fluctuating bulk viscosity implies that Panobinostat induces strong local density variations, possibly due to transient aggregation, solvation shell reorganization, or hydrophobic clustering, all of which hinder volumetric flow. Meanwhile, the steadier shear viscosity indicates less disturbance in directional flow, pointing to more homogeneous resistance in tangential stress. The average value of Bulk and Shear Viscosity is (0.0080 ± 0.0036) and (0.0075 ± 0.0019) (Mean ± S.D) $kgm^{-1}s^{-1}$ respectively, which is significantly higher than that of pure water, confirming that Panobinostat creates a viscous microenvironment. These results provide molecular-level insights that could inform future studies on drug delivery and pharmacokinetics, as increased local viscosity can affect diffusion, bioavailability, and interaction dynamics with biological membranes and proteins. Overall, the graph does not simply quantify viscosity. It reveals the molecular-scale impact of a drug on its surrounding medium, showcasing how deeply it can influence the system's physical behavior.

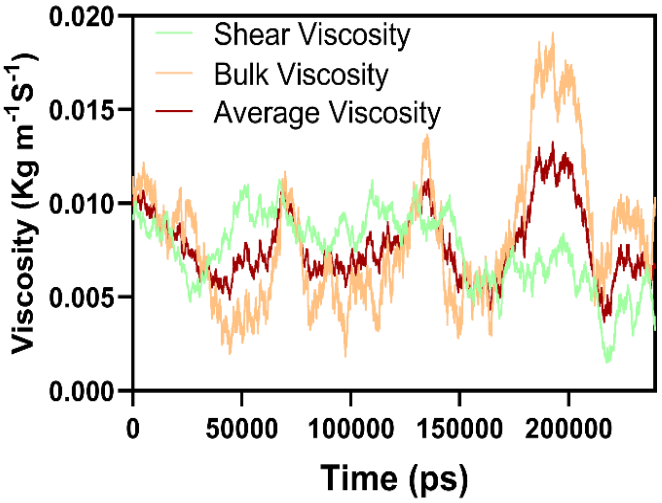

Figure 6: Shear, Bulk and average viscosity of Panobinostat in water at 310 K.

Radial Distribution Function

The radial distribution function (RDF) is used to understand the structural analysis of the system. RDF gives the probability of finding particles around a reference particle. We have investigated RDF between oxygen atoms of water molecules; and the oxygen atoms of water molecules and nitrogen atoms of Panobinostat molecule for crucial structural information about molecular systems. Figure 7(a) shows the water-water RDF. From Table 3 and Figure 7(a), the first peak appears at around 0.28 nm. This indicates that there is strong hydrogen bonding between water molecules. After this sharp peak, the RDF quickly stabilizes to a value near 1, which suggests that the water becomes well-mixed beyond the first hydration shell. Figure 7(b) shows the RDF between oxygen atoms of water molecules and

nitrogen atoms of Panobinostat. We observed multiple peaks between 0.3 nm to 1.3 nm as shown in Table 3 and Figure 7(b). This represents different interactions between oxygen atoms of water and nitrogen atoms of Panobinostat in the simulated system. This plot shows that the RDF stabilizes after 1.22 nm, which indicates that there are uniform distributions at longer distances. This quantifies how the molecules are organized relative to each other, revealing the probability of finding particles at specific distances.

Table 3: Radial distribution function peaks between oxygen atoms in water molecules; and between oxygen atoms of water molecules and nitrogen atoms of Panobinostat.

RDF between					
Oxygen atoms of water Molecule			Oxygen atoms of water molecule and Nitrogen atoms of Panobinostat		
r (nm)	$g_{ow\text{-}ow}(r)$	Peak	r (nm)	$g_{ow\text{-}ow}(r)$	Peak
0.28	2.7	First	0.35	0.78	First
0.64	1.01	Second	0.70	0.95	Second
0.68	1.02	Third	1.22	1.00	Third

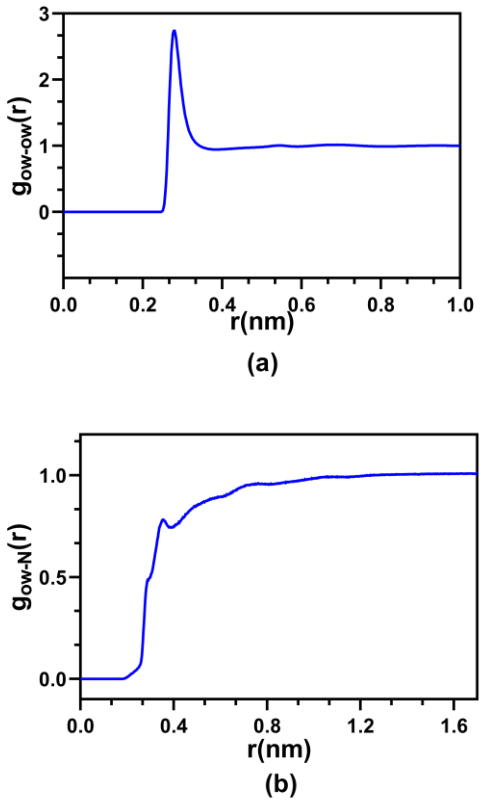

Figure 7: RDF between (a) Oxygen atoms of water molecules, and (b) Oxygen atom of water and Nitrogen atom of Panobinostat at 310 K

CONCLUSIONS

To understand the thermodynamic, transport and structural properties of Panobinostat in water, molecular dynamic study of the system have been carried out at 310 K using GROMACS software. We used charmm36m force field and TIP3P water to model our system. We have estimated the solvation free energy of solute molecule in water using FEP and TI based methods: TI, TI-CUBIC, BAR and MBAR, through the analysis of contributions of Coulomb and vdW interactions to the solvation free energy. The estimated values of solvation free energy using TI, TI-CUBIC, BAR and MBAR methods are 228.78 kJ/mol, 226.97 kJ/mol, 227.68 kJ/mol, and 228.15 kJ/mol respectively. Our results show that Coulomb interaction has major contribution on solvation free energy of the molecules in water. Moreover, we have also analyzed the SASA of the solute molecules as well as hydrogen bond between the solute and solvent molecules to understand the solute-solvent interaction. Almost six hydrogen bonds have been observed throughout simulation; and the hydrogen bonding network greatly impacts on solvation free energy and improves the stability of solvation. Furthermore, both self-diffusion coefficient of solute and solvent molecules as well as their binary diffusion coefficient have been estimated at 310 K temperature through the analysis of MSD followed by the particles using Einstein's and Darken's relation respectively. These results provide the valuable insights of solvation free energy and offer important information for the development of new HDACs inhibitors including improvement of Panobinostat. This also help us to understand the diffusion of HDACs inhibitors. The viscosity is significantly higher than that of pure water that creates a viscous micro-environment. The RDF indicates that there are uniform distributions at longer distances. Future work could explore the effect of temperature variations on these parameters for the comparative analysis with structurally similar molecules.

ACKNOWLEDGMENTS

NG acknowledges the partial PhD grant from Nepal Academy of Science and Technology (NAST).

AUTHOR CONTRIBUTIONS

Conceptualization: NG, NPA; Investigation: NG, NPA; Methodology: NG, NPA; Data curation: NG, NPA; Data analysis: NG, RPK, SPK DA, NPA; Writing - original draft: NG; Writing - review and editing: NG, RPK, SPK, NPA.

CONFLICT OF INTEREST

There is no conflict of interest

REFERENCES

Administration, F. a. D. (2014). *FDA approves Beleodaq to treat rare, aggressive form of non-Hodgkin lymphoma*. Retrieved October 20, 2014 from http://www.fda.gov/NewsEvents/Newsroom/PressAnnouncements/ucm403929.htm

Allen, M. P., & Tildesley, D. J. (2017). *Computer simulation of liquids*. Oxford university press.

Apol, E., Apostolov, R., Berendsen, H., Van Buuren, A., Bjelkmar, P., Van Drunen, R., Feenstra, A., Groenhof, G., Kasson, P., & Larsson, P. (2010). GROMACS user manual version 4.5. 4. *Royal Institute of Technology and Uppsala University, Stockholm*.

Bannan, C. C., Burley, K. H., Chiu, M., Shirts, M. R., Gilson, M. K., & Mobley, D. L. (2016). Blind prediction of cyclohexane–water distribution coefficients from the SAMPL5 challenge. *Journal of computer-aided molecular design, 30*(11), 927-944.

Berendsen, H. J., Postma, J. v., Van Gunsteren, W. F., DiNola, A., & Haak, J. R. (1984). Molecular dynamics with coupling to an external bath. *The Journal of chemical physics, 81*(8), 3684-3690.

Bhandari, D., & Adhikari, N. (2016). Molecular dynamics study of diffusion of krypton in water at different temperatures. *International Journal of Modern Physics B, 30*(11), 1650064.

Bhatta, T., Khanal, P., Khanal, S. P., & Adhikari, N. P. (2023). Thermodynamics and transport properties of valine and cysteine peptides in water. *Journal of Molecular Liquids, 376*, 121472.

Bobo, R. H., Laske, D. W., Akbasak, A., Morrison, P. F., Dedrick, R. L., & Oldfield, E. H. (1994). Convection-enhanced delivery of macromolecules in the brain. *Proceedings of the National Academy of Sciences, 91*(6), 2076-2080.

Bolden, J. E., Peart, M. J., & Johnstone, R. W. (2006). Anticancer activities of histone deacetylase inhibitors. *Nature reviews Drug discovery, 5*(9), 769-784.

Bussi, G., Donadio, D., & Parrinello, M. (2007). Canonical sampling through velocity rescaling. *The Journal of Chemical Physics, 126*(1).

Darken, L. (2010). Diffusion, mobility and their interrelation through free energy in binary metallic systems. *Metallurgical materials transactions. B, Process Metallurgy Materials Processing Science, 41*(2), 277-294.

De Vivo, M., Masetti, M., Bottegoni, G., & Cavalli, A. (2016). Role of molecular dynamics and related methods in drug discovery. *Journal of Medicinal Chemistry, 59*(9), 4035-4061.

Einstein, A. (1905). On the motion of small particles suspended in liquids at rest required by the molecular-kinetic theory of heat. *Annalen der physik, 17*(549-560), 208.

Geballe, M. T., Skillman, A. G., Nicholls, A., Guthrie, J. P., & Taylor, P. J. (2010). The SAMPL2 blind prediction challenge: introduction and overview. *Journal of Computer-aided Molecular Design, 24*(4), 259-279.

Georgalis, Y., Starikov, E., Hollenbach, B., Lurz, R., Scherzinger, E., Saenger, W., Lehrach, H., & Wanker, E. E. (1998). Huntingtin aggregation monitored by dynamic light scattering. *Proceedings of the National Academy of Sciences, 95*(11), 6118-6121.

Giles, F., Fischer, T., Cortes, J., Garcia-Manero, G., Beck, J., Ravandi, F., Masson, E., Rae, P., Laird, G., & Sharma, S. (2006). A phase I study of intravenous LBH589, a novel cinnamic hydroxamic acid analogue histone deacetylase inhibitor, in patients with refractory hematologic malignancies. *Clinical Cancer Research, 12*(15), 4628-4635.

Gill, T., Barua, N., Woolley, M., Bienemann, A., Johnson, D., Murray, G., Fennelly, C., Lewis, O., Irving, C., & Wyatt, M. (2013). In vitro and in vivo testing of a novel recessed-step catheter for reflux-free convection-enhanced drug delivery to the brain. *Journal of Neuroscience Methods, 219*(1), 1-9.

Gromiha, M. M., & Ahmad, S. (2005). Role of solvent accessibility in structure based drug design. *Current Computer-Aided Drug Design, 1*(3), 223-235.

Gryder, B. E., Sodji, Q. H., & Oyelere, A. K. (2012). Targeted cancer therapy: giving histone deacetylase inhibitors all they need to succeed. *Future Medicinal Chemistry, 4*(4), 505-524.

Guthrie, J. P. (2009). A blind challenge for computational solvation free energies:

introduction and overview. *The Journal of Physical Chemistry B, 113*(14), 4501-4507.

Hess, B. (2002). Determining the shear viscosity of model liquids from molecular dynamics simulations. *The Journal of Chemical Physics, 116*(1), 209-217.

Hess, B., Bekker, H., Berendsen, H. J., & Fraaije, J. G. (1997). LINCS: A linear constraint solver for molecular simulations. *Journal of Computational Chemistry, 18*(12), 1463-1472.

Homan, M. J., Franson, A., Ravi, K., Roberts, H., Pai, M. P., Liu, C., He, M., Matvekas, A., Koschmann, C., & Marini, B. L. (2021). Panobinostat penetrates the blood–brain barrier and achieves effective brain concentrations in a murine model. *Cancer Chemotherapy Pharmacology, 88*(3), 555-562.

Huang, J., Rauscher, S., Nawrocki, G., Ran, T., Feig, M., de Groot, B. L., Grubmuller, H., & MacKerell, A. D., Jr. (2017, Jan). CHARMM36m: an improved force field for folded and intrinsically disordered proteins. *Nature Methods, 14*(1), 71-73. https://doi.org/10.1038/nmeth.4067

Humphrey, W., Dalke, A., & Schulten, K. J. (1996). VMD: visual molecular dynamics. *14*(1), 33-38.

Jiang, X.-J., Huang, K.-K., Yang, M., Qiao, L., Wang, Q., Ye, J.-Y., Zhou, H.-S., Yi, Z.-S., Wu, F.-Q., & Wang, Z.-X. (2012). Synergistic effect of panobinostat and bortezomib on chemoresistant acute myelogenous leukemia cells via AKT and NF-κB pathways. *Cancer Letert, 326*(2), 135-142.

Jones, S. F., Bendell, J. C., Infante, J. R., Spigel, D. R., Thompson, D. S., Yardley, D. A., Greco, F. A., Murphy, P. B., & Burris 3rd, H. A. (2011). A phase I study of panobinostat in combination with gemcitabine in the treatment of solid tumors. *Clin Adv Hematol Oncol, 9*(3), 225-230.

Karplus, M., & Petsko, G. A. (1990). Molecular dynamics simulations in biology. *Nature, 347*(6294), 631-639.

Khanal, S. P., & Adhikari, N. P. (2022). Thermodynamic and transport properties of amoxicillin. *Journal of Molecular Liquids, 354*, 118865.

Khanal, S. P., Kandel, Y. P., & Adhikari, N. P. (2019). Transport properties of zwitterion glycine, diglycine, and triglycine in water. *AIP advances, 9*, 065303

Kim, S., Chen, J., Cheng, T., Gindulyte, A., He, J., He, S., Li, Q., Shoemaker, B. A., Thiessen, P. A., & Yu, B. (2025). PubChem 2025 update. *Nucleic Acids Research, 53*(D1), D1516-D1525.

Knox, C., Wilson, M., Klinger, C. M., Franklin, M., Oler, E., Wilson, A., Pon, A., Cox, J., Chin, N. E., & Strawbridge, S. A. (2024). DrugBank 6.0: the DrugBank knowledgebase for 2024. *Nucleic Acids Research, 52*(D1), D1265-D1275.

Kraml, J., Kamenik, A. S., Waibl, F., & Schauperl, M. (2019). Solvation free energy as a measure of hydrophobicity: application to serine protease binding interfaces. *Journal of Chemical Theory Computation, 15*(11), 5872-5882.

Krewson, C. E., & Saltzman, W. M. (1996). Transport and elimination of recombinant human NGF during long-term delivery to the brain. *Brain research, 727*(1-2), 169-181.

Kusaczuk, M., Krętowski, R., Stypułkowska, A., & Cechowska-Pasko, M. (2016). Molecular and cellular effects of a novel hydroxamate-based HDAC inhibitor–belinostat–in glioblastoma cell lines: a preliminary report. *Investigational New Drugs, 34*(5), 552-564.

Lee, J., Cheng, X., Swails, J. M., Yeom, M. S., Eastman, P. K., Lemkul, J. A., Wei, S., Buckner, J., Jeong, J. C., Qi, Y., Jo, S., Pande, V. S., Case, D. A., Brooks, C. L., 3rd, MacKerell, A. D., Jr., Klauda, J. B., & Im, W. (2016). CHARMM-GUI Input Generator for NAMD, GROMACS, AMBER, OpenMM, and CHARMM/OpenMM Simulations Using the CHARMM36 Additive Force Field. *Journal of Chemical Theory Computation, 12*(1), 405-413. https://doi.org/10.1021/acs.jctc.5b00935

Liu, S., Cao, S., Hoang, K., Young, K. L., Paluch, A. S., & Mobley, D. L. (2016). Using MD simulations to calculate how solvents modulate solubility. *Journal of Chemical Theory Computation, 12*(4), 1930-1941.

Maginn, E. J., Messerly, R. A., Carlson, D. J., Roe, D. R., & Elliot, J. R. (2019). Best practices for computing transport properties 1. Self-diffusivity and viscosity from equilibrium molecular dynamics *Living Journal of Computational Molecular Science, 1*(1), 6324-6324.

Morabito, F., Voso, M. T., Hohaus, S., Gentile, M., Vigna, E., Recchia, A. G., Iovino, L., Benedetti, E., Lo-Coco, F., & Galimberti, S. (2016). Panobinostat for the treatment of acute myelogenous leukemia. *Expert Opinion on Investigational Drugs, 25*(9), 1117-1131.

Morrison, P. F., Laske, D. W., Bobo, H., Oldfield, E. H., & Dedrick, R. L. (1994). High-flow microinfusion: tissue penetration and pharmacodynamics. *American Journal of Physiology-Regulatory, Integrative Comparative Physiology, 266*(1), R292-R305.

Pan, D., Mouhieddine, T. H., Upadhyay, R., Casasanta, N., Lee, A., Zubizarreta, N., Moshier, E., & Richter, J. (2023). Outcomes with panobinostat in

heavily pretreated multiple myeloma patients. Seminars in oncology,

Parrinello, M., & Rahman, A. (1981). Polymorphic transitions in single crystals: A new molecular dynamics method. *Journal of Applied Physics, 52*(12), 7182-7190.

Pettersen, E. F., Goddard, T. D., Huang, C. C., Meng, E. C., Couch, G. S., Croll, T. I., Morris, J. H., & Ferrin, T. E. J. P. S. (2021). UCSF ChimeraX: Structure visualization for researchers, educators, and developers. *30*(1), 70-82.

Raedler, L. A. (2016). Farydak (Panobinostat): first HDAC inhibitor approved for patients with relapsed multiple myeloma. *American health drug benefits, 9*(Spec Feature), 84.

Rah, K., & Eu, B. C. (1999). Relation of shear viscosity and self-diffusion coefficient for simple liquids. *Physical Review E, 60*(4), 4105.

Rajak, H., Singh, A., Raghuwanshi, K., Kumar, R., Dewangan, P., Veerasamy, R., Sharma, P., Dixit, A., & Mishra, P. (2014). A structural insight into hydroxamic acid based histone deacetylase inhibitors for the presence of anticancer activity. *Current Medicinal Chemistry, 21*(23), 2642-2664.

Rapaport, D. C. (2004). *The art of molecular dynamics simulation*. Cambridge university press.

Rodgers, L. T., Lester McCully, C. M., Odabas, A., Cruz, R., Peer, C. J., Figg, W. D., & Warren, K. E. (2020). Characterizing the pharmacokinetics of panobinostat in a non-human primate model for the treatment of diffuse intrinsic pontine glioma. *Cancer Chemotherapy Pharmacology, 85*(4), 827-830.

Rosas Jiménez, J. G., Fábián, B., & Hummer, G. (2024). Faster Sampling in Molecular Dynamics Simulations with TIP3P-F Water. *Journal of Chemical Theory Computation, 20*(24), 11068-11081.

San José-Enériz, E., Gimenez-Camino, N., Agirre, X., & Prosper, F. (2019). HDAC inhibitors in acute myeloid leukemia. *Cancers, 11*(11), 1794.

Shirts, M. R., & Chodera, J. D. (2008). Statistically optimal analysis of samples from multiple equilibrium states. *The Journal of Chemical Physics, 129,* 124105.

Shirts, M. R., Mobley, D. L., & Chodera, J. D. (2007). Alchemical free energy calculations: ready for prime time? *Annual Reports in Computational Chemistry, 3*, 41-59.

Shirts, M. R., & Pande, V. S. (2005). Comparison of efficiency and bias of free energies computed by exponential averaging, the Bennett acceptance ratio, and thermodynamic integration. *The Journal of Chemical Physics, 122*, 144107.

Sivaraj, D., Green, M. M., & Gasparetto, C. (2016). Panobinostat for the management of multiple myeloma. *Future oncology, 13*(6), 477-488.

Tsai, P., Wu, G., Baker, C. E., Thayer, W. O., Spagnuolo, R. A., Sanchez, R., Barrett, S., Howell, B., Margolis, D., & Hazuda, D. (2016). In vivo analysis of the effect of panobinostat on cell-associated HIV RNA and DNA levels and latent HIV infection. *Retrovirology, 13*(1), 36.

Tuckerman, M. E. (2023). *Statistical mechanics: theory and molecular simulation*. Oxford university press.

Van Der Spoel, D., Lindahl, E., Hess, B., Groenhof, G., Mark, A. E., & Berendsen, H. J. (2005). GROMACS: fast, flexible, and free. *Journal of Computational Chemistry, 26*(16), 1701-1718.

Wu, D., & Kofke, D. A. (2005). Phase-space overlap measures. II. Design and implementation of staging methods for free-energy calculations. *The Journal of Chemical Physics, 123*, 084109.

Zwanzig, R. W. (1954). High-temperature equation of state by a perturbation method. I. Nonpolar gases. *The Journal of Chemical Physics, 22*(8), 1420-1426.